ELSEVIER

Journal of Nuclear Materials 280 (2000) 196–205

journal of nuclear materials

www.elsevier.nl/locate/jnucmat

Single-pass flow-through experiments on a simulated waste glass in alkaline media at 40°C. I. Experiments conducted at variable solution flow rate to glass surface area ratio

P.K. Abraitis [a,*], B.P. McGrail [b], D.P. Trivedi [c], F.R. Livens [d], D.J. Vaughan [a]

[a] *Department of Earth Sciences, University of Manchester, Williamson Building, Oxford Road, Manchester M13 9PL, UK*
[b] *Applied Geology and Geochemistry Department, Pacific Northwest National Laboratory, Richland, WA 99352, USA*
[c] *British Nuclear Fuels plc, Environmental Assessments, Risley, Warrington, Cheshire WA3 6AS, UK*
[d] *Department of Chemistry, University of Manchester, Oxford Road, Manchester M13 9PL, UK*

Received 11 November 1999; accepted 6 March 2000

Abstract

Dissolution of a borosilicate glass containing a complex mixture of simulated fission product oxides has been investigated in single-pass flow-through (SPFT) experiments in moderately alkaline media at 40°C. The experiments were designed such that the ratio of the solution flow rate to the glass surface area varied extensively over the experimental matrix. Dissolution of the glass is surface reaction-controlled under these experimental conditions. In Si-rich, alkaline solutions, the concentration of Al is moderated to very low levels by the development of secondary aluminosilicate gels. Rates of dissolution decrease linearly as the solution activity product $a_{\mathrm{Al(OH)_4^-\,(aq)}}{}^{0.06} a_{\mathrm{H_4SiO_4^0}}{}^{0.51}$ increases. A rate law containing a mixed Al/Si affinity term gives good agreement with the experimental data. © 2000 Elsevier Science B.V. All rights reserved.

PACS: 21.41.Kw; 82.55.+e; 82.20.wt; 82.70.Gg

1. Introduction

It is important to understand how key environmental variables affect the rates of glass dissolution in order to predict the performance of nuclear waste glasses in repository systems. Glass dissolution models aim to account for the effects of important rate-influencing variables such as temperature, pH and solution composition. To be successful, these models must be based on a sound mechanistic understanding of the dissolution process.

Many current models include a rate law based on the transition state theory (TST) of reaction rates [1]. A generalised form of such a rate law that is applicable to surface reaction-controlled processes has been given by Lasaga [2]. This takes the form

$$\text{Rate} = k_0 S\, \mathrm{e}^{-E_a/RT} a_{\mathrm{H^+}}^{n_{\mathrm{H^+}}} g(I) \prod_i a_i^{n_i} f(\Delta G_r), \tag{1}$$

where k_0 is the intrinsic rate constant, S the reactive surface area, E_a the activation energy, RT the product of the gas constant and the absolute temperature, $a_{\mathrm{H^+}}$ the hydronium ion activity, $n_{\mathrm{H^+}}$ the reaction order with respect to $a_{\mathrm{H^+}}$, and $g(I)$ is a term accounting for the ionic strength dependence of the reaction; the product term $\prod_i a_i^{n_i}$ describes the net catalytic or inhibitory effects of rate-influencing species (other than the hydronium ion) and the final term $f(\Delta G_r)$ is a free energy function describing the reaction rate dependence on the deviation from equilibrium (a reaction affinity term).

* Corresponding author. Tel.: +44-161 275 7489; fax: +44-161 275 3947.
E-mail address: pabraitis@fs1.ge.man.ac.uk (P.K. Abraitis).

PII: S0022-3115(00)00041-6

For the purposes of glass dissolution modelling a simplified TST rate law has been employed by numerous authors [3–8]. The general form of the rate law is

$$\text{Rate}_i = k_0 v_i \, e^{-E_a/RT} a_{H^+}^n \left[1 - \left(\frac{Q}{K}\right)^{\sigma}\right], \quad (2)$$

where Rate_i is the release rate of glass component i, v_i the stoichiometric coefficient for element i, Q the activity product of the rate-limiting reaction and K the equilibrium constant for this reaction, and σ is the overall reaction order. Here, the only species which is assumed to catalyse (or inhibit) the rate of dissolution is H^+. The final square bracketed term describes the thermodynamic reaction affinity.

The presence of an affinity term in such rate laws implies that reactions governing dissolution are reversible, such that a state of thermodynamic equilibrium is possible [2]. At equilibrium, rates of dissolution and precipitation are equal and a zero net dissolution rate is predicted. The form of the affinity function is rarely elementary (as in Eq. (2)) even in the case of relatively simple mineral phases, such as gibbsite and kaolinite [9,10].

For glasses, the overall dissolution process is irreversible and no overall equilibrium is attainable. Here it is assumed that there is a reversible microscopic reaction that is rate limiting. Grambow [3] suggested that the rate-limiting reaction is the hydrolysis of siloxane bonds and Q is defined as $a_{H_4SiO_4}$ (the activity of silicic acid) and K is $a_{H_4SiO_4}$ at saturation.

More recently, rates laws have been proposed which include elements other than Si. Bourcier et al. [11] suggest an affinity term involving the saturation state with respect to a secondary amorphous gel containing Si, Fe, Al, Ca and Mg. Gin [5] suggested that a mixed Al/Si affinity term is appropriate for modelling dissolution kinetics of the French 'R7T7' glass. Daux et al. [6] propose a rate law for a basaltic glass which includes Si, Fe and Al. Advocat et al. [7] propose a rate law for the SON68 glass that includes all glass components in the affinity term.

Few studies have systematically investigated and quantified the catalytic or inhibitory effects of aqueous species (other than H^+), even though such effects are potentially important. Dissolution of silica polymorphs is governed by siloxane hydrolysis reactions and rates of dissolution are catalysed by aqueous cations such as Na^+ (aq) [12] and inhibited by a variety of metals including Al [13], Fe, Zn, Cu, Be and Ga [14]. It has been suggested that silicic acid may inhibit dissolution of a borosilicate glass in addition to contributing to the reaction affinity [7]. The presence of lead was found to significantly inhibit the dissolution of a borosilicate glass and this effect was rationalised on the basis of chemisorption of Pb at reactive sites [15]. Dissolution rates in the presence of Pb were 2 orders of magnitude lower than those in systems where Pb was absent. This effect has no reaction 'affinity' basis since Pb was not present in the glass. Catalysis is also possible and accelerated glass dissolution has been widely reported in the presence of organic acid ligands (particularly those containing two or more functional groups) (e.g. [16,17]).

Many glass dissolution models are based on the results of batch dissolution tests. As discussed by Bourcier [4], model parameters are often obtained from the same experiments to which the model is applied. It is not surprising that a multiple parameter model (such as Eq. (2)) can be fit to batch experimental data. The fact that an excellent fit may be obtained does not necessarily indicate that the model is a correct approximation of the underlying physical processes.

From an experimental viewpoint, determination of many parameters in such models is problematic. Firstly, the rate of glass dissolution is typically fast enough that it is experimentally difficult to maintain solute concentrations below levels likely to result in secondary product precipitation and to maintain 'far from saturation' conditions [2]. Secondly, it is difficult to distinguish between catalytic/inhibitory effects and potential contributions to the affinity term for glass-derived species. Few studies, such as that of McGrail et al. [18], have systematically isolated the effects of individual rate-influencing factors and presented formal methods for parameter estimation from well-constrained experimental data.

In this study, we have investigated the dissolution rate of a borosilicate glass containing a complex mixture of simulated fission product oxides. Single-pass flow-through (SPFT) experiments [18] have been conducted at 40°C in alkaline media (a KOH/KCl buffer solution). Experiments have been geared to investigating the specific role of aqueous Si and Al species during glass dissolution since both elements have been shown to influence glass dissolution rates. The experiments were designed to isolate, as far as possible, the effects of varying dissolved Al and Si concentrations at constant pH and temperature.

Part I presents the results of SPFT experiments in which the solution flow rate and glass surface area were systematically varied across the experimental matrix. In this approach, the same input buffer solution is used in each experiment and the solution composition is only influenced by glass/solution reactions and secondary processes, such as the development of solid reaction products. Part II presents the results of experiments where the same solution flow rate to glass surface area ratio was used with different input buffer compositions. In these experiments, the input buffers have been systematically spiked with Si and Al in an attempt to isolate the rate-influencing effects of these elements. Results are compared with predictions based on a number of rate law formulations.

2. Experimental methodology

2.1. Glass samples

A non-radioactive glass was used in this study. This comprised a Li–Mg–Na–Al–Fe bearing borosilicate containing a complex mixture of simulated fission product oxides. The chemical composition of the glass (as determined by analysis) may be expressed using the formula

$$Al_{0.0630}B_{0.3333}Ba_{0.0020}Ca_{0.0001}Ce_{0.0034}Cr_{0.0042}Cs_{0.0023}Fe_{0.0175}Hf_{0.0001}K_{0.0003}La_{0.0017}Li_{0.1773}Mg_{0.0772}Mo_{0.0073}Na_{0.1647}Nd_{0.0057}Ni_{0.0001}P_{0.0015}Rb_{0.0007}Ru_{0.0017}Pr_{0.0017}Si_{0.5149}Sm_{0.0010}S_{0.0008}Sr_{0.0019}Te_{0.0006}Ti_{0.0001}Y_{0.0011}Zn_{0.0083}Zr_{0.0038}O_{1.9725}$$

Experiments were performed with a single batch of glass powder prepared from bulk glass blocks according to standard product consistency test (PCT) methods [19]. Following crushing, the glass powder was size fractionated by sieving. The 150–75 μm (−100 + 200 mesh) fraction was utilised in all experiments following ultrasonic cleaning in water and absolute ethanol. The surface area of this glass powder was estimated geometrically at 205 $cm^2\ g^{-1}$.

2.2. Single-pass flow-through experiments

The design of the apparatus is shown schematically in Fig. 1. These experiments, designated MW-F_1–MW-F_15, utilised an alkaline buffer comprising a solution of 0.00018 M KOH (Apache Chemicals) + 0.005 M KCl (Baker). The modelled pH of this buffer (in the absence of dissolved CO_2) is 10.22 at 25°C and 9.76 at 40°C (all solution speciation modelling was conducted with the PHREEQC code [20]).

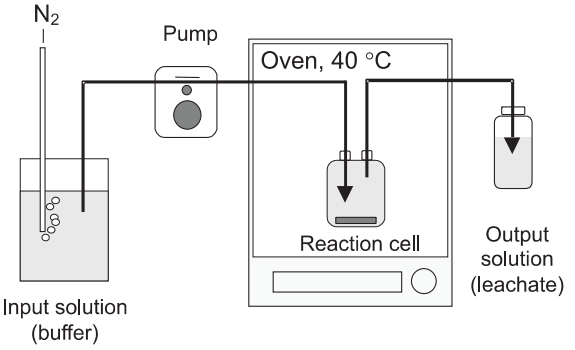

Fig. 1. Schematic diagram of the SPFT apparatus used in this study. The diagram shows the apparatus comprising a single experiment. Sixteen such experiments were performed simultaneously.

The reaction cells comprise Savillex polytetrafluoroethane (PTFE) containers with an internal volume of 60 ml. Input buffer solution is held within a solution reservoir. The headspace above the input buffer solution was purged with a nitrogen stream and the solution was continuously pumped through the two-port reaction cells with peristaltic pumps (Ismatec). Reaction cells were located within an oven that was maintained at 40°C. The reaction cell output solution was delivered into a sample collection vessel.

This experimental design permitted independent control over flow rates and buffer compositions and 16 independent tests were conducted in each set of experiments. Experiments were conducted at 40°C for 19 d and five samples were collected during the course of each test. The mass of the collection vessel was recorded at each sampling point to permit flow rate determination. The experiments were designed such that the range of flow rate (q, $m^3\ s^{-1}$) per unit glass surface area (s, m^2) ratios varied considerably between tests. The variation in $\log_{10}(q/s)$ spanned 3.31 log units across the experimental matrix. Within a given test, flow rate variation ranged from <0.5% relative standard deviation (RSD) at the highest flow rates to 13% RSD at the lowest flow rates.

Samples of the reaction cell output solutions were collected for analysis and pH measurement at room temperature. A number of the output solutions in the MW-F experiments were filtered through 1.8 nm (pore size) Centriflo membrane ultrafiltration cones prior to analysis. There was no evidence of colloid formation in these tests since the concentrations of Al, B, Li, Mg, Na and Si in ultrafiltered (<1.8 nm) glass leachate samples were identical within experimental error to those in the corresponding unfiltered samples.

Samples of the output solutions were acidified to 1% nitric acid (Fisher Ultrex grade) for analysis by ICP–AES. Only the major glass components Al, B, Fe, Li, Mg, Na and Si were determined in the solutions since the solubility of many minor glass components (such as the lanthanides and Zr) is very low at this pH. Blank samples of the input buffer solution were collected and analysed in each test. Analytical uncertainty was less than 3% RSD in most cases. However, Al and Fe concentrations were close to detection limits in some tests, and greater analytical uncertainty (RSD $\leqslant$ 10%) was associated with these analytes. In the MW-F_13–MW-F_15 tests the concentration of Al was below 20 ppb (which is the practical ICP–AES detection limit in this solution matrix).

2.3. Selective extraction of reacted glass powders

Following removal from the reaction vessels at the end of the experiments, the reacted glass powders were rinsed with deionised water and dried at 40°C. Samples

of the unreacted glass and selected samples from the MW-F experiments were subjected to two selective extraction procedures which are designed to dissolve hydrous gels such as those found in soils [21].

Samples were treated with an ammonium oxalate/oxalic acid reagent at pH 3. Samples of dried glass (0.025 g) were treated with 20 ml of the reagent for 4 h in the dark. Samples were also treated with an alkaline carbonate reagent [21]. Here, duplicate samples of dried glass (0.025 g) were treated with 20 ml of 0.5 M K_2CO_3 for 18 h in the dark. Solutions were continuously mixed during the extraction procedure with magnetic stir bars. Each extract was filtered (using 0.22 μm pore size cellulose nitrate filters) and acidified to 2% HNO_3 for analysis by ICP–AES.

2.4. Rate determination

Normalised dissolution rates have been calculated in units of grams of glass dissolved per square metre per day (g m^{-2} d^{-1}). Boron concentrations are used to estimate the extent of dissolution since this element is highly soluble and not readily incorporated in secondary reaction products. Rates were determined on the basis of 'steady-state' output concentrations and calculated using the formula [18]

$$R_{i,j} = (C_{i,j} - C_{i,\mathrm{B}})\frac{q_j}{v_i s_j}, \tag{3}$$

where $R_{i,j}$ is the normalised dissolution rate (g m^{-2} d^{-1}) based on the ith element at the jth sampling, q_j (m^3 s^{-1}) the flow rate at time j, $C_{i,j}$ the concentration of component i at the jth sampling, $C_{i,\mathrm{B}}$ the background concentration of component i, v_i the mass fraction of component i in the glass, and s_j (m^2) is the average surface area over the time period $j-1$ to j. All rate calculations were performed using a dedicated database and data analysis code. Changes in the surface area of the glass during the experiment were estimated using the method described by McGrail et al. [18]. In the majority of cases, such surface area corrections were negligible.

A correction factor has been applied to the rate values, to adjust the measured rates to those predicted at pH 9.38 which was the 'mean' solution pH based on the average measured $a\mathrm{H}^+$ in each experiment (including the experiments described in Part II). This correction factor was developed assuming that B release rates are proportional to $a_{\mathrm{H}^+}^{-0.41}$ in alkaline media [22]. The correction factor is given by

$$\mathrm{Rf} = \left(\frac{10^{-9.38}}{10^{-\mathrm{pH}(i)}}\right)^{-0.41}. \tag{4}$$

Here, Rf is the rate correction factor and pH(i) is the solution pH at 40°C. Due to the narrow pH range in the MW-F experiments this factor varied only slightly (ranging from 1.091 to 1.265).

3. Results and discussion

3.1. Solution compositions and modelling

The reaction cell output concentrations were time dependent, as shown in Fig. 2. Following commencement of the tests, the concentrations of glass-derived solutes vary with time until a steady-state situation is attained. Flow rates ranged from 1.74 to 111 ml d^{-1}. At the highest flow rates, steady-state is attained rapidly and the concentration of B in the reaction cell output solutions was essentially constant from 3 d onwards. At lower flow rates, steady-state conditions were observed after approximately 9 d.

The solution chemistry data are presented in Table 1 as the mean concentrations (mg l^{-1}) of each analyte as measured in the final three leachate samples collected from each reaction cell.

The pH of the freshly prepared buffer solution (0.00018 M KOH + 0.005 M KCl) was 10.25 at room temperature. The modelled pH of this basic buffer solution is 10.22 at 25°C and 9.76 at 40°C, so the experimental pH is expected to be 0.46 pH units lower than that measured at 25°C. During the experiments, samples of the input buffer were collected periodically for pH measurement. Measured pH values ranged from 9.65 to 9.74 over the 19-d period. This is lower than the modelled pH at room temperature and is also lower than the pH of freshly prepared buffer. The modelled pH of the buffer at equilibrium with atmospheric CO_2 partial pressures ($\mathrm{pCO_2} = -3.5$) is 7.54 at 25°C. The modelled pH of the buffer in equilibrium with $\mathrm{pCO_2} = -6.0$ is 9.72 at 25°C, which is in reasonable agreement with the measured pH values. It would appear that the buffer pH values may be influenced by diffusion of CO_2 into the buffer reservoir or that traces of CO_2 may be present in the N_2 gas supply.

To interpret the results of these experiments it is important to assess the distribution of important Si and Al solution species in the reaction cell solutions. The pH of the input buffer solutions varied between 9.60 and 9.75. In basic solutions, Si may be present in the form of both monosilicate species and as complex polysilicates, the former dominating in mildly alkaline, dilute Si solutions [23]. Monosilicic acid is dibasic, with $\mathrm{p}K_1 = 9.84$ and $\mathrm{p}K_2 = 13.43$ at 25°C and infinite solution dilution [23]. At this pH, monosilicate species comprising orthosilicic acid and the conjugate bases $H_3SiO_4^-$ (aq) and $H_2SiO_4^{2-}$ (aq) are the major silica species (orthosilicic acid and the $H_3SiO_4^-$ (aq) anion being dominant). The major Al species is the tetrahydroxoaluminate anion ($Al(OH)_4^-$ (aq)); over 99% of the Al atoms in solution are predicted to be present in this form.

A simple geochemical modelling approach has been adopted to predict the speciation of Al and Si in the reaction cell solutions. Firstly, it is assumed that the

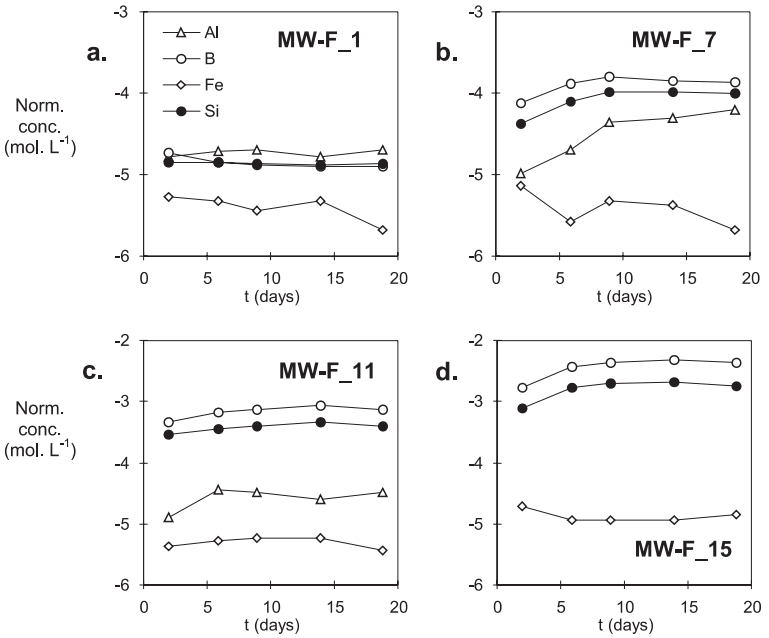

Fig. 2. The normalised molar concentrations of Al, B, Si and Fe versus time during the MW-F experiments at: (a) $\log_{10} q/s$ (m s^{-1}) = −5.92; (b) $\log_{10} q/s$ (m s^{-1}) = −7.27; (c) $\log_{10} q/s$ (m s^{-1}) = −8.12; (d) $\log_{10} q/s$ (m s^{-1}) = −9.22.

Table 1
Solution chemistry data from the MW-F experiments[a]

Experiment	Al	B	Fe	Li	Mg	Na	Si
MW-F_1	0.062	0.090	0.007	0.034	0.055	0.158	0.381
MW-F_2	0.104	0.165	0.007	0.061	0.096	0.227	0.656
MW-F_3	0.169	0.271	0.006	0.101	0.158	0.363	1.067
MW-F_4	0.158	0.326	0.005	0.123	0.182	0.433	1.258
MW-F_5	0.191	0.528	0.012	0.193	0.264	0.656	1.918
MW-F_6	0.183	0.741	0.009	0.275	0.347	0.902	2.438
MW-F_7	0.172	1.045	0.007	0.382	0.447	1.199	2.933
MW-F_8	0.246	1.907	0.010	0.726	0.836	2.273	5.280
MW-F_9	0.163	2.457	0.012	0.874	1.001	2.640	6.307
MW-F_10	0.125	3.813	0.037	1.335	1.448	4.033	8.837
MW-F_11	0.100	5.390	0.010	1.929	1.903	5.720	11.81
MW-F_12	0.078	8.763	0.010	3.029	2.523	9.057	17.27
MW-F_13	<DL	12.39	0.024	4.565	3.634	14.01	24.16
MW-F_14	<DL	17.31	0.023	6.204	4.217	19.40	31.83
MW-F_15	<DL	31.17	0.024	10.96	5.672	34.43	55.00

[a] All values are mean concentrations (mg l^{-1}) based on analyses of samples of the reaction cell output solutions taken after 8.9, 13.9 and 18.8 d. Note that Al was below the 20 μg l^{-1} detection limit (<DL) in a number of the tests.

solution pH in the reaction cells is 0.46 pH units lower than the measured buffer pH in each case. For modelling purposes, the analytically determined solution concentrations of Al, B, Fe, Li, Mg, Na and Si were input, together with the buffer 'recipe' concentrations of additional solution components such as EDTA, chloride and nitrate. In the speciation model, the solution pH was constrained to the estimated pH at 40°C by addition of KOH to the model solution in order to attain charge balance.

3.2. Congruence of the dissolution process

In Fig. 3, rates of glass dissolution based on the major glass components (Si, B, Li, Mg, and Al) are

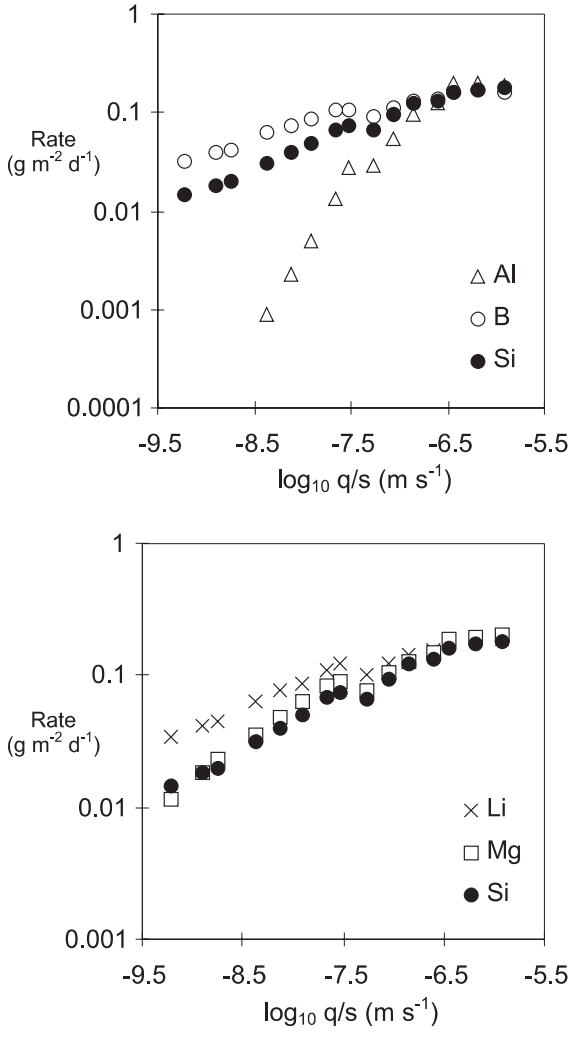

Fig. 3. Normalised dissolution rates based on Al, B, Li, Mg and Si steady-state concentrations versus $\log_{10} q/s$ (m s^{-1}).

plotted versus the $\log_{10}$ of the q/s ratio (which varied between -5.92 and -9.22 in these experiments, see Table 2).

Equivalent rates are obtained on the basis of the concentrations of each element in the tests conducted with $\log_{10} q/s > -6.5$. This indicates that the dissolution process is essentially congruent under these experimental conditions (at least for these major glass components). Congruent dissolution of this glass in alkaline media has also been observed in alkaline pH-buffered batch dissolution experiments [22].

At lower $\log_{10} q/s$ values Al, Mg and Si rates are significantly lower than those based on B and Li. The solubility of Fe(III) oxyhydroxides is low at this pH and Fe concentrations were lower than those predicted on the basis of congruent glass dissolution in each test. Note that Al concentrations were below the ICP–AES detection limits (20 ppb) in MW-F_13, MW-F_14 and MW-F_15 experiments.

3.3. Secondary phase development

The congruence trends shown in Fig. 3 may be explained if secondary phases containing Si, Mg, Al and Fe are developing in the reaction vessels.

Geochemical modelling of the solution chemistry data suggests that the systems are oversaturated with respect to a wide variety of *potential* secondary phases. In Fig. 4, saturation indices for selected phases are plotted versus $\log_{10} (q/s)$ ratios. Quartz and chalcedony are supersaturated in a number of the tests. Amorphous silica is undersaturated in all experiments. Saturation with respect to silica gel is approached in the MW-F_15 experiment. Goethite is supersaturated in each experiment and saturation indices for amorphous ferric hydroxide are close to zero. Diaspore is supersaturated in all experiments where Al was detected in the leachates whilst gibbsite is undersaturated in each case. Aluminosilicate minerals including clay minerals (K-bearing montmorillonites, sepiolite, talc and kaolinite) and a zeolite (phillipsite) are supersaturated in many of the solutions.

Scanning electron microscopic examination did not reveal the existence of any visible secondary phases at the surfaces of the reacted glass powders. However, energy dispersive analysis of the glass revealed the presence of potassium. This element was not detected by EDS in the unreacted glass. This suggests that K was incorporated into the glass (or secondary products near the glass surface) during reaction with the KOH/KCl buffer solution.

To investigate the possibility of hydrous secondary gel development, a number of samples of the reacted glasses were treated using selective extractant reagents (as described in Section 2.3). For comparison, samples of the unreacted glass were also treated using these reagents.

The amount of an element extracted from the samples during the procedure is expressed in units of normalised extracted moles, calculated using the expression

$$\mathrm{NEM}_i = ([i]_{\mathrm{Sample}} - [i]_{\mathrm{Glass}})\mathrm{Sf}^i \frac{m_{\mathrm{Sample}}}{m_{\mathrm{Extracted}}}. \quad (5)$$

Here, $[i]_{\mathrm{Sample}}$ is the concentration of the element i in an extract of the reacted glass sample (mol l^{-1}), $[i]_{\mathrm{Glass}}$ the concentration of the element in an equivalent extract of the unreacted glass powder (mol l^{-1}), Sf^i the stoichiometric factor for element i (defined as the ratio of the number of moles of Si to the number of moles of the element i in the glass), m_{Sample} is the mass of glass (g) that was present in the reaction cell during the SPFT experiment and $m_{\mathrm{Extracted}}$ is the mass of glass (g) used in the

Table 2
Data from the MW-F experiments

Test ID	$\log_{10} q/s$ (m s^{-1})	pH[a]	Rf[b]	Rate (g m^{-2} d^{-1})[c]	$a_{Al(OH)_4^-}$ [d]	$a_{H_4SiO_4}$ [d]
MW-F_1	−5.92	9.74	1.102	0.164 ± 0.012	2.14×10^{-6}	9.14×10^{-6}
MW-F_2	−6.19	9.75	1.096	0.170 ± 0.027	3.55×10^{-6}	1.56×10^{-5}
MW-F_3	−6.44	9.71	1.139	0.166 ± 0.032	5.78×10^{-6}	2.61×10^{-5}
MW-F_4	−6.60	9.72	1.124	0.139 ± 0.034	5.40×10^{-6}	3.06×10^{-5}
MW-F_5	−6.85	9.66	1.186	0.134 ± 0.030	6.53×10^{-6}	4.86×10^{-5}
MW-F_6	−7.06	9.69	1.158	0.115 ± 0.025	6.27×10^{-6}	6.01×10^{-5}
MW-F_7	−7.27	9.75	1.093	0.091 ± 0.017	5.90×10^{-6}	6.94×10^{-5}
MW-F_8	−7.53	9.61	1.247	0.108 ± 0.027	8.41×10^{-6}	1.38×10^{-4}
MW-F_9	−7.66	9.60	1.265	0.105 ± 0.029	6.03×10^{-6}	1.66×10^{-4}
MW-F_10	−7.91	9.66	1.192	0.086 ± 0.022	4.26×10^{-6}	2.24×10^{-4}
MW-F_11	−8.12	9.70	1.148	0.072 ± 0.018	3.42×10^{-6}	2.91×10^{-4}
MW-F_12	−8.37	9.75	1.091	0.064 ± 0.023	2.65×10^{-6}	4.10×10^{-4}
MW-F_13	−8.74	9.67	1.179	0.042 ± 0.024	<DL[e]	6.07×10^{-4}
MW-F_14	−8.90	9.67	1.174	0.040 ± 0.022	<DL[e]	7.97×10^{-4}
MW-F_15	−9.22	9.70	1.144	0.033 ± 0.006	<DL[e]	1.35×10^{-3}

[a] Estimated pH at 40°C, given by the measured pH (at room temperature) minus 0.46 pH units.
[b] Rate correction factor (calculated using Eq. (4)).
[c] Mean pH corrected rate of glass dissolution based on steady-state boron output concentrations. Uncertainties are 95% confidence limits ($n = 3$).
[d] Activities modelled using PHREEQC [20].
[e] Al concentrations less than the detection limit (20 ppb).

selective extraction procedure ($m_{Extracted}$ was 0.025 ± 0.002 g in each case).

Fig. 5(a) shows NEM_i values for Al, B, Fe, Li, Mg and Si obtained using the 0.5 M K_2CO_3 reagent. The composition of the extracts of the MW-F_2 glass was similar to that obtained for the fresh glass samples. The results for the other glasses indicate that a carbonate-soluble secondary material, enriched in Al, Fe, Mg and Si and depleted in B and Li, is present at the surface of these samples.

Fig. 5(b) shows NEM_i values for Al, B, Fe, Li, Mg and Si extracted from reacted samples using the pH 3 ammonium oxalate/oxalic acid reagent. The acid oxalate reagent resulted in more extensive dissolution than the carbonate reagent. Element concentrations in the acid extracts were between three and 10 times higher than those obtained using the alkaline carbonate solution. The data suggest that an Al-enriched, B-depleted acid oxalate soluble fraction is present in the MW-F_11 and MW-F_15 samples. Results obtained using the acid oxalate reagent are less conclusive, possibly because this reagent was less selective and caused more extensive dissolution of both the gel and unreacted glass.

Potassium concentrations were also determined in the acid oxalate extract solutions. Bulk analysis of the fresh glass revealed the presence of trace quantities of K (0.01% (w/w) K_2O). Small amounts of K were extracted from the fresh glass and the MW-F_2 reacted glass samples. Considerably larger amounts of K were present in the acid oxalate extracts of the other glass samples. This indicates that a K-enriched, acid oxalate soluble fraction has developed during these experiments.

These findings, coupled with the reaction cell output solution compositions, are consistent with the formation of a K-bearing secondary gel in these systems. From these data it is unclear if the material comprises a single 'gel' or a mixture of discrete hydroxide or hydrosilicate phases. Fe concentrations in all experiments were lower than those predicted on the basis of congruent dissolution, so it would appear than a Fe-bearing phase (such as ferrihydrite or amorphous ferric hydroxide) largely controlled Fe concentrations in these tests. No crystalline secondary mineral phases were identified.

3.4. Factors influencing the dissolution rates

Table 2 presents glass dissolution rates in the MW-F experiments based on boron concentrations in the reaction cell output solutions. These rate data may be compared with predictions made on the basis of a number of glass dissolution models.

3.4.1. Surface reaction or transport-controlled dissolution

Flow rates varied significantly between experiments, ranging from 1.74 to 111 ml d^{-1}. If dissolution of this glass is influenced by the rate of reaction product transport away from the reacting surfaces (i.e., if dissolution is transport controlled [24]), then rates of dissolution would be predicted to increase with the solution mixing rate.

A number of tests were performed at a variety of flow rates to investigate this possibility. Parallel experiments were conducted at identical flow rate and glass surface

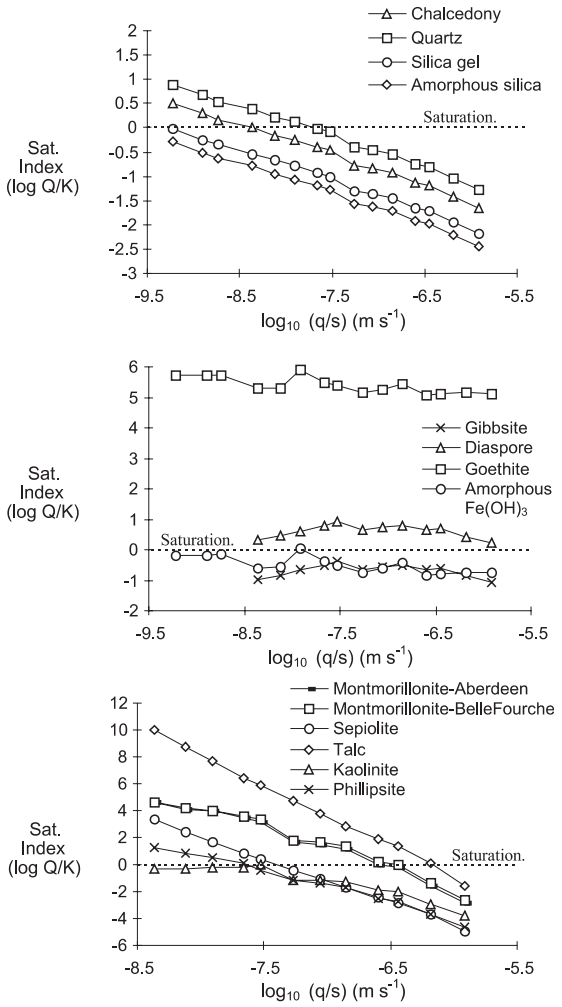

Montmorillonite-Aberdeen = $(H,Na,K)_{0.14}Mg_{0.45}Fe_{0.33}Al_{1.47}Si_{3.82}O_{10}(OH)_2$

Montmorillonite-BelleFourche = $(H,Na,K)_{0.09}Mg_{0.29}Fe_{0.24}Al_{1.57}Si_{3.93}O_{10}(OH)_2$

Fig. 4. Computed saturation indices for selected potential secondary phases in the MW-F experiments versus $\log_{10} q/s$ (m s^{-1}).

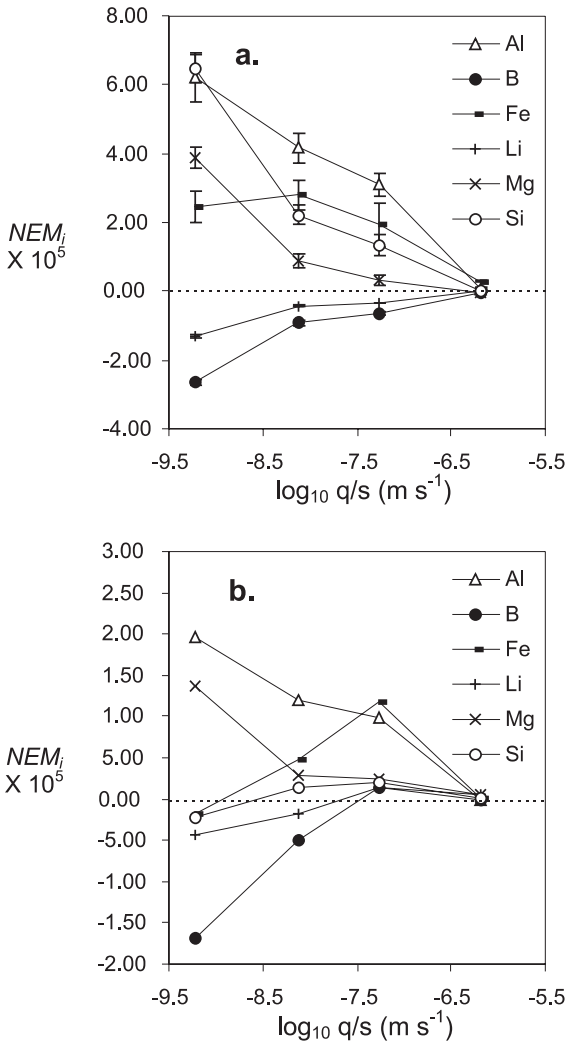

Fig. 5. NEM_i values for Al, B, Fe, Mg and Si versus $\log_{10} q/s$ (m s^{-1}): (a) selective extraction in a 0.5 M K_2CO_3 solution (error bars are sample standard deviations based on duplicate extractions); (b) selective extraction in a pH 3 oxalic acid/ammonium oxalate solution.

area. In one cell the solution was continuously stirred whilst the other cell was not actively mixed (as in the MW-F experiments). In each case, the reaction cell output solutions contained concentrations of all glass-derived solutes that were equal within experimental error. This confirms that the dissolution process is not influenced by the solution mixing rate and supports the hypothesis that dissolution is governed by surface reactions under these experimental conditions. Apparent activation energies associated with the dissolution of this glass in alkaline media are also consistent with a surface reaction-controlled dissolution process [22].

3.4.2. The influence of dissolved silica

Fig. 6 shows the steady-state glass dissolution rate versus the activity of orthosilicic acid. It is clear that the rates do not show a linear dependence on the activity of this species. Therefore, a rate law including an affinity term dependent only on the activity of orthosilicic acid, such as that in the model proposed by Grambow [3], does not provide an adequate fit to the experimental data.

In order to fit these data to the rate law proposed by Grambow [3], a non-unity value of σ (the Tempkin coefficient, as defined in Eq. (2)) is required. This approach has been suggested by Bourcier et al. [25] in a study based on static dissolution experiments with a

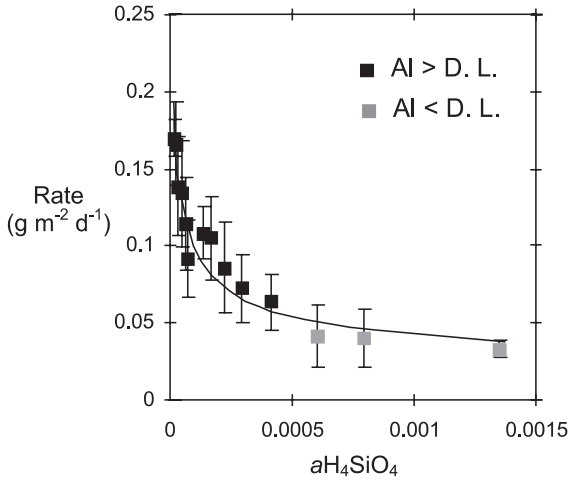

Fig. 6. Rates of glass dissolution (based on steady-state B concentrations) versus the activity of orthosilicic acid in the MW-F experiments. Error bars are 95% confidence limits ($n = 3$). The curve is a best fit trendline based on a power law ($\text{Rate} = xa\text{H}_4\text{SiO}_4^n$). Note that Al was below ICP–AES detection limits in three of the tests (Al < DL).

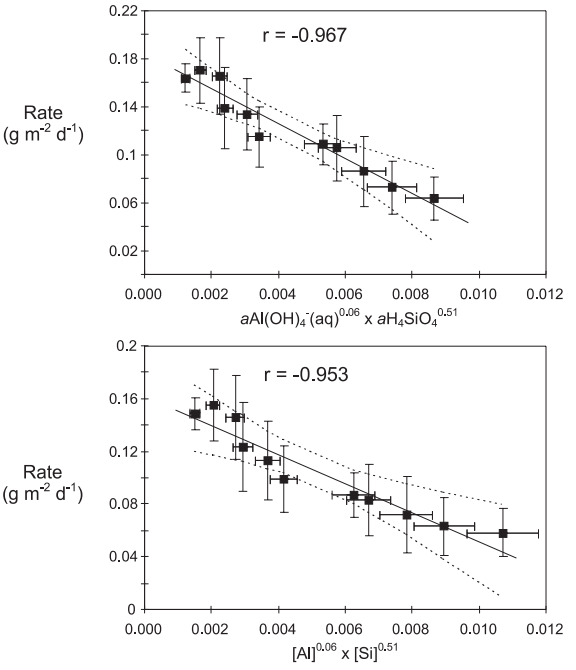

Fig. 7. Rates of glass dissolution (based on steady-state B concentrations) in the MW-F experiments. Ordinate error bars are 95% confidence limits ($n = 3$) and abscissa error bars are ±10%. Data relating to the MW-F_13–MW-F_15 experiments are not shown since Al was below detection limits. The plots show (a) pH-corrected rates versus the activity product term $a_{\text{Al(OH)}_4^-\,(\text{aq})}{}^{0.06} \cdot a_{\text{H}_4\text{SiO}_4}{}^{0.51}$, and (b) non-pH-corrected rates versus the molar concentration product term $[\text{Al}]^{0.06} \cdot [\text{Si}]^{0.51}$. The dashed lines are 95% confidence limits about the regression line and r values are the product moment correlation coefficients.

borosilicate glass. However, as discussed in the next section and in Part II, the experimental data indicate that both dissolved Si and Al influence the dissolution rate of this glass.

3.4.3. Combined influence of dissolved silica and aluminate species

In Fig. 7(a), the pH-corrected experimental dissolution rate data are plotted versus the activity product $a\text{Al(OH)}_4^-\,(\text{aq})^{0.06} \cdot a\text{H}_4\text{SiO}_4^{0.51}$. The exponent values 0.06 and 0.51 are the mole fractions of Al and Si in the MW glass, respectively. Note that data from the MW-F_13–MW-F_15 experiments are not included in Fig. 7 because Al was below ICP–AES detection limits in the reaction cell output solutions.

The data indicate that there is a strong negative linear correlation between the experimental rates and this activity product (the product moment correlation coefficient $(r) = -0.967$), suggesting that a mixed Al/Si rate law is appropriate. The experimental rates in the MW-F experiments therefore appear to be consistent with the following rate law formulation:

$$R = R_0\left(1 - \frac{a^{0.06}_{\text{Al(OH)}_4^-\,(\text{aq})}\, a^{0.51}_{\text{H}_4\text{SiO}_4}}{K_{\text{Al·Si}}}\right), \tag{6}$$

where R is the rate of glass dissolution (g m^{-2} d^{-1}), R_0 the apparent rate constant under these experimental conditions (40°C, pH 9.38) and $K_{\text{Al·Si}}$ is a constant defined as the activity product $a_{\text{Al(OH)}_4^-\,(\text{aq})}{}^{0.06} a_{\text{H}_4\text{SiO}_4}{}^{0.51}$ which corresponds to a hypothetical zero rate of dissolution (which has not been observed experimentally). Values of R_0 and $K_{\text{Al·Si}}$ estimated from these data by linear regression are $R_0 = 0.183 \pm 0.006$ g m^{-2} d^{-1} and $K_{\text{Al·Si}} = 0.012 \pm 0.001$.

Given the combined uncertainties in the estimated pH at 40°C, the modelled activities of $\text{Al(OH)}_4^-\,(\text{aq})$ and H_4SiO_4 and the pH-corrected rates, it is useful to consider the raw concentration data and non-pH-corrected rate values. Fig. 7(b) shows the non-pH-corrected experimental dissolution rates plotted versus the molar concentration product $[\text{Al}]^{0.06} \cdot [\text{Si}]^{0.51}$. The rate and measured concentration data shown in this plot are not subject to the additional uncertainties introduced by the geochemical modelling calculations and the rate pH correction procedure. This plot shows a similar trend to that in Fig. 7(a), further illustrating the dissolution rate dependence on the combined Al/Si affinity term. A concentration-dependent rate law that is consistent with these data takes the form

$$R = R_0\left(1 - \frac{[\text{Al}]^{0.06}[\text{Si}]^{0.51}}{K_{\text{Al·Si}}}\right), \tag{7}$$

where R is the rate of glass dissolution (g m^{-2} d^{-1}), R_0 the apparent rate constant and $K_{Al\cdot Si}$ is a constant defined as the molar concentration product $[Al]^{0.06}[Si]^{0.51}$ which corresponds to a hypothetical zero rate of dissolution. Values of R_0 and $K_{Al\cdot Si}$ estimated from these data by linear regression are $R_0 = 0.162 \pm 0.007$ g m^{-2} d^{-1} and $K_{Al\cdot Si} = 0.014 \pm 0.001$. A strong negative linear correlation between the non-pH-corrected rates and this molar concentration product is observed ($r = -0.953$).

Thus, under these experimental conditions, a TST rate law containing a combined Al/Si affinity term provides good agreement with the experimental rate data. Gin [5] also found that a rate law containing a mixed Al/Si reaction affinity term of this type gave good agreement to data obtained in flow-through experiments with the R7T7 glass. In the alkaline, Si-rich solutions that develop in the low q/s ratio experiments described here, development of secondary hydrosilicate gels controls dissolved Al concentrations to very low levels (below 20 μg l^{-1}). Due to the development of these aluminosilicate secondary phases it is highly unlikely that 'saturation' will be reached.

4. Conclusions

SPFT experiments with a complex borosilicate waste glass have revealed that dissolution is congruent and surface reaction-controlled at 40°C in moderately alkaline media. Secondary gels develop under test conditions where significant quantities of glass-derived solutes accumulate in the leachate. These gels contain Si, Mg, Al and Fe. Gel development controls Al concentrations to very low levels.

A glass dissolution rate law including an affinity term containing a mixed Al/Si activity product formulation provided the best agreement with the experimental data. In the context of the TST, these results are consistent with the formation of an activated complex containing Al and Si in the same molar ratio as that present in the bulk glass. Additional experiments are described in Part II of this publication to further investigate the role of dissolved Al and Si species in determining glass dissolution rates.

Acknowledgements

This work was conducted at the Battelle Pacific Northwest National Laboratory (PNNL) and was financially supported by British Nuclear Fuels plc. and Associated Western Universities, Inc., under a grant with the US Department of Energy.

References

[1] A.C. Lasaga, in: A.C. Lasaga, R.J. Kirkpatrick (Eds.), Kinetics of Geochemical Processes, Reviews in Mineralogy 8, 1981, p. 135 (Chapter 4).
[2] A.C. Lasaga, in: A.F. White, S.L. Brantley (Eds.), Chemical Weathering Rates of Silicate Minerals, Reviews in Mineralogy 31, 1995, p. 23 (Chapter 2).
[3] B. Grambow, Mater. Res. Symp. Proc. 44 (1985) 209.
[4] W.L. Bourcier, Mater. Res. Soc. Symp. Proc. 333 (1994) 69.
[5] S. Gin, Mater. Res. Symp. Proc. 412 (1996) 189.
[6] V. Daux, C. Guy, T. Advocat, J.L. Crovisier, P. Stille, Chem. Geol. 142 (1997) 109.
[7] T. Advocat, J.L. Chouchan, J.L. Crovisier, C. Guy, V. Daux, C. Jegou, S. Gin, E. Vernaz, Mater. Res. Symp. Proc. 506 (1998) 63.
[8] G. Berger, C. Claparols, C. Guy, V. Daux, Geochim. Cosmochim. Acta 58 (1994) 4875.
[9] K.L. Nagy, A.C. Lasaga, Geochim. Cosmochim. Acta 56 (1992) 3093.
[10] K.L. Nagy, A.E. Blum, A.C. Lasaga, Am. J. Sci. 291 (1991) 649.
[11] W.L. Bourcier, D.W. Peiffer, K.G. Knauss, K.D. McKeegan, D.K. Smith, Mater. Res. Symp. Proc. 176 (1990) 209.
[12] G. Berger, E. Cadore, J. Schott, P.M. Dove, Geochim. Cosmochim. Acta 58 (1994) 541.
[13] R. Iler, J. Colloid Interface Sci. 43 (1973) 399.
[14] P.M. Dove, in: A.F. White, S.L. Brantley (Eds.), Chemical Weathering Rates of Silicate Minerals, Reviews in Mineralogy 31, 1995, p. 235 (Chapter 6).
[15] C.Q. Buckwalter, L.R. Pederson, J. Am. Ceram. Soc. 65 (1982) 431.
[16] S. Gin, N. Godon, J.P. Mestre, E.Y. Vernaz, Appl. Geochem. 9 (1994) 255.
[17] H. Teng, D.E. Grandstaff, Mater. Res. Soc. Symp. Proc. 412 (1996) 249.
[18] B.P. McGrail, W.L. Ebert, A.J. Bakel, D.K. Peeler, J. Nucl. Mater. 249 (1997) 175.
[19] ASTM, Standard test methods for determining the chemical durability of nuclear waste glasses: the product consistency test (PCT), ASTM C1285-94, Annual Book of ASTM Standards, Philadelphia, PA, 1994.
[20] D.L. Parkhurst, Water-Resources Investigations Report 95-4227, US Geological Survey, 1995.
[21] B.F.L. Smith, in: M.J. Wilson (Ed.), Clay Mineralogy: Spectroscopic and Chemical Determinative Methods, 1994, p. 331 (Chapter 9).
[22] P.K. Abraitis, D.J. Vaughan, F.R. Livens, J. Monteith, D.P. Trivedi, J.S. Small, Mater. Res. Symp. Proc. 506 (1998) 47.
[23] S. Sjoberg, J. Non-Cryst. Solids 196 (1996) 51.
[24] R.A. Berner, in: A.C. Lasaga, R.J. Kirkpatrick (Eds.), Kinetics of Geochemical Processes, Reviews in Mineralogy 8, 1981, p. 111 (Chapter 3).
[25] W.L. Bourcier, S.A. Carroll, B.L. Phillips, Mater. Res. Symp. Proc. 333 (1994) 507.